Dynamic cell cycle–dependent phosphorylation modulates CENP-L–CENP-N centromere recruitment

Alexandra P. Navarro[a,b] and Iain M. Cheeseman[a,b,*]
[a]Whitehead Institute for Biomedical Research, Cambridge, MA 02142; [b]Department of Biology, Massachusetts Institute of Technology, Cambridge, MA 02142

ABSTRACT **The kinetochore is a macromolecular structure that is needed to ensure proper chromosome segregation during each cellular division. The kinetochore is assembled upon a platform of the 16-subunit constitutive centromere-associated network (CCAN), which is present at centromeres throughout the cell cycle. The nature and regulation of CCAN assembly, interactions, and dynamics needed to facilitate changing centromere properties and requirements remain to be fully elucidated. The CENP-LN complex is a CCAN component that displays unique cell cycle–dependent localization behavior, peaking in the S phase. Here, we demonstrate that phosphorylation of CENP-L and CENP-N controls CENP-LN complex formation and localization in a cell cycle–dependent manner. Mimicking constitutive phosphorylation of either CENP-L or CENP-N or simultaneously preventing phosphorylation of both proteins prevents CENP-LN localization and disrupts chromosome segregation. Our work suggests that cycles of phosphorylation and dephosphorylation are critical for CENP-LN complex recruitment and dynamics at kinetochores to enable cell cycle–dependent CCAN reorganization.**

Monitoring Editor
Kerry Bloom
University of North Carolina, Chapel Hill

Received: Jun 30, 2022
Accepted: Jul 7, 2022

INTRODUCTION

The kinetochore plays a critical role in ensuring the fidelity of chromosome segregation during each cell division (Cheeseman, 2014). Kinetochore assembly is restricted to the centromere of each chromosome due to the presence of a centromere-specific histone H3 variant called CENP-A. Within the inner kinetochore, the 16-subunit complex constitutive centromere-associated network (CCAN) functions to recognize CENP-A. These inner kinetochore proteins are defined by their constitutive assembly at centromeres throughout all phases of the cell cycle (Navarro and Cheeseman, 2021). The CCAN, in turn, provides a platform for assembly of the outer kinetochore, which ultimately binds to spindle microtubules to facilitate chromosome segregation. The proteins of the CCAN are canonically grouped into five sub-complexes: CENP-C, CENP-LN, CENP-HIKM, CENP-TWSX, and CENP-OPQUR (Earnshaw and Rothfield, 1985; Saitoh *et al.*, 1992; Foltz *et al.*, 2006; Okada *et al.*, 2006; Hori *et al.*, 2008b; Amano *et al.*, 2009; Carroll *et al.*, 2009; Nishino *et al.*, 2012; Basilico *et al.*, 2014; Weir *et al.*, 2016). Of these proteins, CENP-C and CENP-N recognize and bind to CENP-A directly (Carroll *et al.*, 2009; Guse *et al.*, 2011; Kato *et al.*, 2013; Falk *et al.*, 2015; Allu *et al.*, 2019). CCAN assembly relies on interdependent interactions between these protein complexes such that the absence of one protein at centromeres results in the misvocalization of other inner kinetochore sub-complexes (Okada *et al.*, 2006; Hori *et al.*, 2008a; Basilico *et al.*, 2014; McKinley *et al.*, 2015).

Although the inner kinetochore is localized constitutively to centromeres, the structure and organization of this protein assembly changes in a cell cycle-dependent manner (Navarro and Cheeseman, 2020). First, centromeres undergo a significant structural change during G2 and upon entry into mitosis, when the inner kinetochore proteins CENP-C and CENP-T serve as a binding site for outer kinetochore recruitment (Cheeseman *et al.*, 2008; Gascoigne and Cheeseman, 2013; Malvezzi *et al.*, 2013). Outer

This article was published online ahead of print in MBoC in Press (http://www.molbiolcell.org/cgi/doi/10.1091/mbc.E22-06-0239) on July 13, 2022.

*Address correspondence to: Iain M. Cheeseman (icheese@wi.mit.edu).

Abbreviations used: ACA, anti-centromere antibody; CCAN, constitutive centromere-associated network; BSA, bovine serum albumin; CDK, cyclin dependent kinase; CENP, centromere protein; CRISPR, clustered regularly interspaced short palindromic repeats; DM1a, alpha tubulin antibody; DTT, dithiothreitol; EDTA, ethylenediamine tetraacetic acid; EGTA, ethylene glycol-bis(β-aminoethyl ether)-*N,N,N′,N′*-tetraacetic acid; FACS, fluorescence-activated cell sorting; FBS, fetal bovine serum; GFP, green fluorescent protein; HEPES-N-2, hydroxyethylpiperazine-*N′*-2-ethanesulfonic acid; iKO, inducible knock out; LAP, localization and affinity purification; m, monomeric; MeOH, methanol; MCS, multiple cloning site; PBS, phosphate-buffered saline; RFP, red fluorescent protein; sgRNA, single guide RNA; TCEP, tris(2-carboxyethyl)phosphine; Td, tandem dimer; WT, wild type.

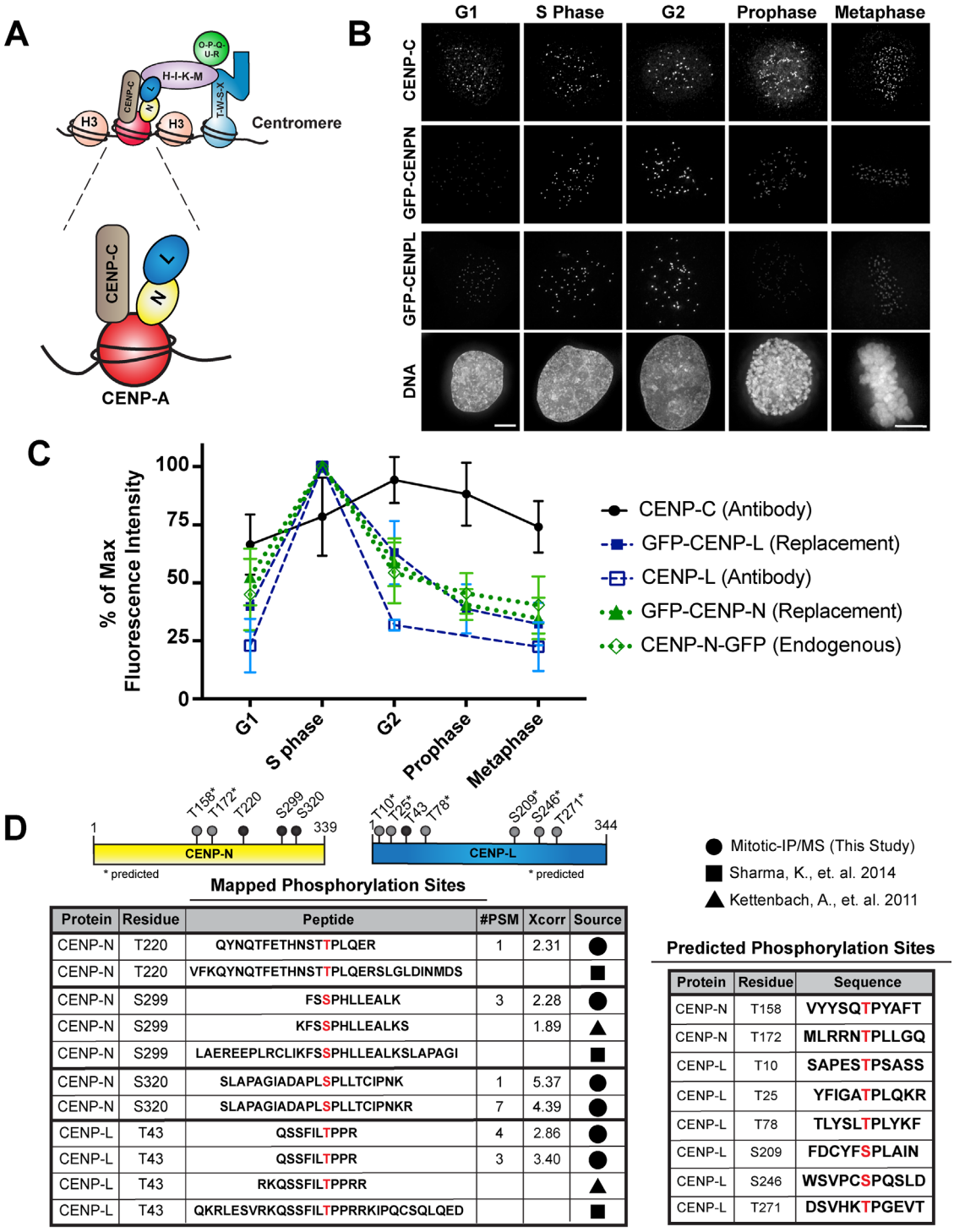

Protein	Residue	Peptide	#PSM	Xcorr	Source
CENP-N	T220	QYNQTFETHNSTTPLQER	1	2.31	●
CENP-N	T220	VFKQYNQTFETHNSTTPLQERSLGLDINMDS			■
CENP-N	S299	FSSPHLLEALK	3	2.28	●
CENP-N	S299	KFSSPHLLEALKS		1.89	▲
CENP-N	S299	LAEREEPLRCLIKFSSPHLLEALKSLAPAGI			■
CENP-N	S320	SLAPAGIADAPLSPLLTCIPNK	1	5.37	●
CENP-N	S320	SLAPAGIADAPLSPLLTCIPNKR	7	4.39	●
CENP-L	T43	QSSFILTPPR	4	2.86	●
CENP-L	T43	QSSFILTPPR	3	3.40	●
CENP-L	T43	RKQSSFILTPPRR			▲
CENP-L	T43	QKRLESVRKQSSFILTPPRRKIPQCSQLQED			■

Predicted Phosphorylation Sites

Protein	Residue	Sequence
CENP-N	T158	VYYSQTPYAFT
CENP-N	T172	MLRRNTPLLGQ
CENP-L	T10	SAPESTPSASS
CENP-L	T25	YFIGATPLQKR
CENP-L	T78	TLYSLTPLYKF
CENP-L	S209	FDCYFSPLAIN
CENP-L	S246	WSVPCSPQSLD
CENP-L	T271	DSVHKTPGEVT

FIGURE 1: CENP-N and CENP-L levels vary throughout the cell cycle. (A) Diagram illustrating the proteins that interact directly with centromere histone, CENP-A, within the constitutive centromere-associated network (CCAN). (B) Representative images of centromere protein levels throughout the cell cycle. All GFP images are scaled to the S-phase image for each corresponding row. *Note:* The signal intensity in the representative images for G2 represents centromeres that have not been resolved following duplication of centromere DNA. Therefore, the signal in these images is brighter than what is represented in the quantification. DNA images shown in this figure are taken from the GFP-CENP-L cells shown in this image. Scale bar is 5 μm. (C) Quantification of CENP-C, CENP-N, and CENP-L levels throughout the cell cycle. CENP-C levels were detected using an antibody against CENP-C. CENP-N and CENP-L levels were determined using replacement cell lines expressing GFP-tagged transgenes. Additionally, CENP-L levels were determined using an antibody against untagged endogenous CENP-L a HeLa cell line not expressing GFP-CENP-L cell cycle stages were determined using the following markers: G1/prophase/mitosis–DM1a (presence of midbody for G1); spindle morphology for prophase and mitosis; S phase–PCNA (selected cells specifically in mid–S phase) Schonenberger *et al.*, 2015; G2–cyclin B (looked for cytoplasmic Cyclin-B signal). Fluorescence intensity is graphed as a percent of max fluorescence. Each dot in the graph

kinetochore assembly is restricted to mitosis due to the requirement for phosphorylation of CENP-C and CENP-T by mitotic kinases (Gascoigne *et al.*, 2011; Screpanti *et al.*, 2011; Huis In 't Veld *et al.*, 2016; Pekgoz Altunkaya *et al.*, 2016). Coupled with this change in kinetochore architecture, the interdependent relationships between CCAN subcomplexes also change. For example, during interphase, CENP-C relies on its interaction with CENP-LN and CENP-HIKM for its centromere localization, whereas during mitosis, CENP-C can localize to kinetochores in the absence of other CCAN subcomplexes (McKinley *et al.*, 2015; Nagpal *et al.*, 2015). This change is mediated in part by the phosphorylation of CENP-C in mitosis by cyclin-dependent kinase (CDK), which acts to increase the affinity of CENP-C for CENP-A and thereby promotes its association with kinetochores independent of its association with other CCAN components (Watanabe *et al.*, 2019). Together, these regulated changes in kinetochore organization indicate that molecular reorganization occurs within the inner kinetochore between interphase and mitosis. However, how the other proteins of the inner kinetochore adapt to these changes has not been fully elucidated.

The CENP-L/N complex plays a critical role in the assembly of the inner kinetochore as it binds directly to both CENP-A and other CCAN components. Although CENP-N and CENP-L are thought to interact stably, each protein performs a specific function within this complex. The N-terminus of CENP-N interacts directly with a distinct loop within CENP-A and this interaction is sufficient to recruit CENP-N to centromeres during interphase (Carroll *et al.*, 2009, 2010; Fang *et al.*, 2015; McKinley *et al.*, 2015; Guo *et al.*, 2017; Pentakota *et al.*, 2017; Chittori *et al.*, 2018; Tian *et al.*, 2018; Allu *et al.*, 2019). The C-terminus of CENP-N interacts directly with CENP-L and through this interaction binds to CENP-C and CENP-HIKM (Carroll *et al.*, 2009; Hinshaw and Harrison, 2013; McKinley *et al.*, 2015; Pentakota *et al.*, 2017). Together, CENP-N and CENP-L effectively bridge the interface between centromere chromatin and the assembled CCAN. However, CENP-N levels at kinetochores decrease in mitosis. Recent structural models have suggested that mitotic kinetochores contain sub stoichiometric amounts of CENP-N relative to interphase (Hellwig *et al.*, 2008; Fang *et al.*, 2015; Allu *et al.*, 2019). Here, we show that CENP-N and CENP-L are phosphorylated in mitosis and that mimicking constitutive phosphorylation at these phosphorylation sites is sufficient to prevent kinetochore localization and disrupt the interaction between CENP-N and CENP-L. The dynamic nature of this phosphorylation event is critical, as mutants that fully prevent CENP-LN complex phosphorylation also disrupt its kinetochore recruitment. This work highlights the molecular changes that occur within the inner kinetochore throughout the cell cycle and helps reveal the features that enable a functional mitotic kinetochore assembly state.

RESULTS AND DISCUSSION

CENP-L/N kinetochore localization decreases upon entry into mitosis

To assess changes in the organization of the inner kinetochore throughout the cell cycle, we sought to quantify the localization of inner kinetochore components that interact directly with the centromere histone, CENP-A (Figure 1A). Based on antibody staining and reference cell cycle markers to determine the corresponding cell cycle stage (Supplemental Figure 1A), we found that CENP-C levels remain relatively constant throughout the cell cycle (Figure 1, B and C), consistent with prior work (Gascoigne and Cheeseman, 2013). Prior studies analyzing endogenous CENP-N localization have been limited by the nature of the available CENP-N antibodies. Therefore, we assessed CENP-N localization in cells stably expressing N-terminally tagged GFP-CENP-N as the only CENP-N species present using a CRISPR/Cas9-based replacement strategy to deplete endogenous CENP-N (see (McKinley *et al.*, 2015)) or using C-terminally tagged CENP-N tagged at its endogenous locus. In contrast to CENP-C, CENP-N was enriched during S phase, but then decreased as cells progressed to mitosis (Figure 1, B and C; Supplemental Figure 1A), consistent with prior work (Allu *et al.*, 2019; Fang *et al.*, 2015; Hellwig *et al.*, 2011). Within the CCAN, CENP-N forms an obligate complex with CENP-L (Figure 1A). To assess CENP-L levels, we utilized a similar replacement assay using a cell line expressing a GFP-CENP-L fusion in a CENP-L inducible knockout background. In addition, we used an antibody against the endogenous CENP-L protein. Similarly to CENP-N, we found that CENP-L was enriched at kinetochores in the S phase followed by reduction to 30% relative of its maximal enrichment upon entry into mitosis (Figure 1, B and C). The increased levels of CENP-N and CENP-L at S-phase kinetochores coincides with the cell cycle stage during which new molecules of CENP-N are recruited to centromeres (Fang *et al.*, 2015; Hellwig *et al.*, 2011). Therefore, whereas CENP-C levels remain constant throughout the cell cycle, CENP-N and CENP-L kinetochore localization is enriched at S phase but reduced upon entry into mitosis.

CENP-L and CENP-N are phosphorylated in mitosis

The reduced localization of the CENP-L/N complex in mitosis suggests that this complex undergoes cell cycle–specific changes that alter its centromere localization. Based on the prevalent role of post-translational modifications in regulating diverse aspects of kinetochore assembly and function (Hara and Fukagawa, 2020; Navarro and Cheeseman, 2020), we hypothesized that CENP-N and CENP-L may be post translationally modified in a cell cycle–dependent manner. To test this, we isolated GFP-CENP-N from cells enriched either in mitosis or in S phase and GFP-CENP-L from mitotically enriched cells by immunoprecipitation. Our mass spectrometry analysis identified established interacting partners for CENP-N and CENP-L from both S phase and mitotically-enriched samples (Supplemental Figure 1, B and C). In addition, we identified phosphorylation sites in CENP-N and CENP-L that were present specifically in samples isolated from mitotic cells (Figure 1D; Supplemental Figure 1D). These sites have also been identified in proteome-wide mass spectrometry studies as being enriched in mitotic cells (Kettenbach *et al.*, 2011; Sharma *et al.*, 2014; Hornbeck *et al.*, 2015; Figure 1D). We note that the sequence composition of CENP-N and CENP-L precludes the ability to identify tryptic peptides spanning their entire sequence using standard mass spectrometry approaches (see Peptide Atlas—https://db.systemsbiology.net/), so that there are likely to be additional phosphorylation

represents the mean percentage of max fluorescence intensity value obtained from three separate experiments. In each experiment 5, 10, and 10 cells were imaged per cell cycle stage and at least 40 kinetochores were quantified per cell. (D) Tables representing the mapped and predicted phosphorylation sites for CENP-N and CENP-L. Phosphorylation sites mapped by mass spectrometry include results from my data and previously published data of mitotically enriched proteomewide mass spectrometry analysis. The figure legend indicates where the phosphopeptides were identified. Predicted phosphorylation sites are additional serine/threonine residues in both CENP-L and CENP-N that fit the minimal CDK consensus sequence [S/T]-P. PSM = peptide spectrum match; X_{corr} = cross-correlation.

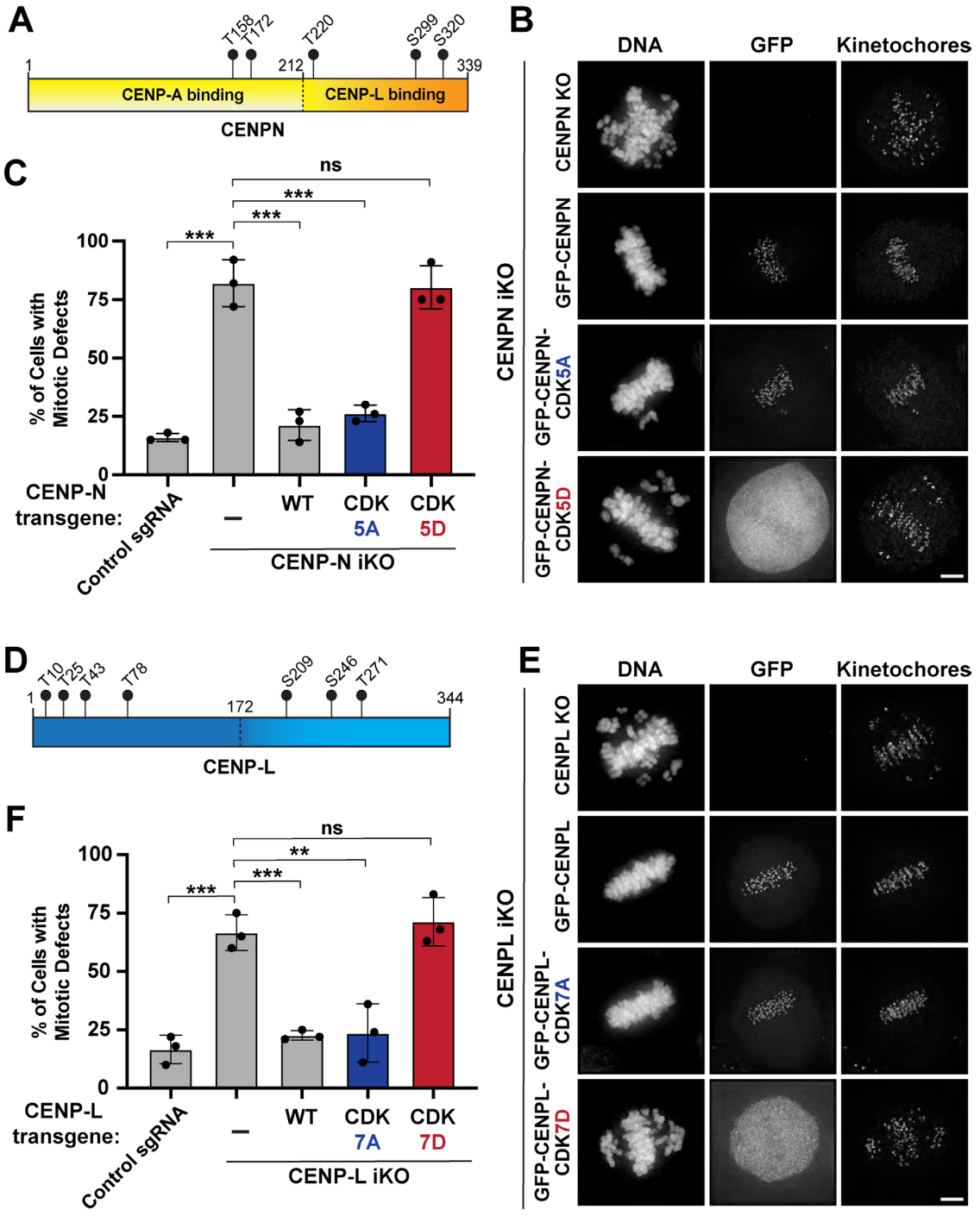

FIGURE 2: Mutating phosphorylation sites in CENP-L and CENP-N affect their ability to localize to the kinetochore. (A) Diagram illustrating the positions of the SP/TP sites that were mutagenized in the CDK phosphomutants of CENP-N. We specifically note the sites that are present in the two known functional domains of CENP-N. (B) Representative images of the mitotic phenotypes observed for each replacement condition. All images were deconvolved and max projected. Images are scaled the same. Scale bar is 5 μm. (C) Quantification of mitotic phenotypes in CENP-N replacement cell lines after 5-day induction of endogenous CENP-N in the inducible knockout (iKO) cell line. Each point in the graph represents the percentage of cells with mitotic defects in three separate experiments. In each experiment at least 100 mitotic cells were randomly assessed for mitotic defects using microtubule stain to identify cells in mitosis (not shown). Multiple clones for each cell line were assessed to similar results-data shown was collected from a single clone over three experiments. The control sgRNA used is a guide that cuts a single time in the genome (van den Berg *et al.*, 2018). Error bars indicate SD. Unpaired two-tailed *t* test was performed. *p* values from left to right: *** = 0.0004, *** = 0.0009, *** = 0.0008, ns = 0.8424. (D) Diagram illustrating the positions of the SP/TP sites that were mutagenized in the CDK-phosphomutants of CENP-L. (E) Representative images of the mitotic phenotypes observed for each replacement condition. All images were deconvolved and max projected. Images are scaled the same. Scale bar is 5 μm. (F) Quantification of mitotic phenotypes in CENP-L replacement cell lines after 5-day induction of endogenous CENP-L

events beyond those identified here and in prior work. Interestingly, the majority of the phosphorylation sites identified in CENP-N and CENP-L correspond to a minimal cyclin-dependent kinase (CDK) consensus sequence (ps/pT-[P]; ps/pT-[P]-X-R; Songyang *et al.*, 1994; Figure 1D). Together, our mass spectrometry data indicate that both CENP-N and CENP-L are phosphorylated in mitosis.

Phosphorylation affects CENP-N and CENP-L function

We next sought to investigate whether the phosphorylation sites we identified in both CENP-L and CENP-N contribute to their function. To do this, we generated phosphomutants for both proteins. For these studies, we mutated all the CDK consensus sites present in either protein including those that were not mapped in our IP-mass spec analysis (Figure 1D; Figure 2, A and D). Importantly, many of these SP/TP sites are conserved in other vertebrate CENP-L and CENP-N orthologs (Supplemental Figure 2, A and B). To test the consequences of preventing phosphorylation, we mutated each serine or threonine residue to alanine (referred to as CENP-N$^{CDK\text{-}5A}$ and CENP-L$^{CDK\text{-}7A}$ mutants). Reciprocally, to mimic constitutive phosphorylation at these CDK consensus sites, we mutated each serine or threonine to aspartate (CENP-N$^{CDK\text{-}5D}$ or CENP-L$^{CDK\text{-}7D}$ mutants). Depletion of CENP-N and CENP-L using a Cas9-inducible knockout strategy with a single guide RNA (sgRNA) targeting the corresponding gene results in severe chromosome misalignment (McKinley *et al.*, 2015; Figure 2, B and E). This phenotype was rescued by the expression of wild-type GFP-tagged transgenes hardened against the corresponding sgRNA sequence (Figure 2, B, C, E, and F). Similarly, we found that phosphonull mutants of either CENP-N$^{CDK\text{-}5A}$ or CENP-L$^{CDK\text{-}7A}$ localized to kinetochores and were able to support proper chromosome alignment and segregation in the absence of the endogenous protein, with only modest mitotic phenotypes (Figure 2, B, C, E, and F). However, in the presence of the endogenous CENP-N protein, we found that the CENP-N$^{CDK\text{-}5A}$ mutant displayed substantially reduced kinetochore localization during both interphase and mitosis (Supplemental Figure 3A). This suggests that the CENP-N$^{CDK\text{-}5A}$ mutant cannot compete fully with the endogenous protein for its localization to kinetochores.

In contrast to these relatively modest phenotypes in the absence of CDK phosphorylation, we found that mutants mimicking the constitutively phosphorylated state displayed substantial mitotic defects. Both CENP-N$^{CDK\text{-}5D}$ and CENP-L$^{CDK\text{-}7D}$ were unable to localize to kinetochores and failed to rescue proper chromosome segregation (Figure 2, B, C, E, and F). Given the different localization behavior of the CENP-N and CENP-L phosphomutants, we assessed the localization of other CCAN proteins under these different replacement conditions. With the exception of CENP-C, which continued to localize when endogenous CENP-N and CENP-L were depleted, all other CCAN proteins failed to localize in mutants in which CENP-L or CENP-N were delocalized from kinetochores (Supplemental Figure 3, B and C; also see McKinley *et al.*, 2015). This suggests that these phosphomutants disrupt the proper assembly of the inner kinetochore. We additionally tested mutants in phosphorylation sites identified in our mass spectrometry analysis that did not correspond to a CDK consensus site (Supplemental Figure 1D). However, phosphomutants targeting these non-CDK sites for CENP-N did not show a change in localization behavior or function (unpublished data). Together, these results suggest that the phosphorylation state of either CENP-L or CENP-N affects its ability to localize to kinetochores so that mimicking constitutive phosphorylation disrupts kinetochore function for either protein.

Phosphorylation affects the interaction between CENP-L and CENP-N

Previous work has found that CENP-L and CENP-N are interdependent for their localization to kinetochores (McKinley *et al.*, 2015; Pentakota *et al.*, 2017). Given that phosphomimetic versions of CENP-L or CENP-N prevented their kinetochore localization (Figure 2, B and E), we hypothesized that phosphorylation of these residues could regulate the interaction between CENP-L and CENP-N or their interactions with other CCAN proteins. To evaluate this, we assessed recently published CCAN structures (Pesenti *et al.*, 2022; Yatskevich *et al.*, 2022). Consistent with the potential of these CDK consensus phosphorylation sites to regulate protein interactions, we found that a subset of these residues were present at the interface between CENP-N and CENP-L (Figure 3). In addition, other CDK consensus phosphorylation sites were present at interfaces between CENP-L or CENP-N with other CCAN proteins, including the CENP-HIKM and CENP-OPQUR complexes.

Based on the potential for phosphorylation of these CDK consensus-motif residues to alter protein interactions, we sought to test these interactions in the presence of phosphomimetic mutations. To do this, we took a cell-based approach by adapting a previously established *lacO*-tethering assay (Gascoigne *et al.*, 2011). For this assay, we utilized a U2OS cell line that has a stably integrated *lacO* array on chromosome 1 (Gascoigne *et al.*, 2011; Janicki *et al.*, 2004). We then transiently coexpressed a bait construct tagged with LacI-GFP that binds with high affinity to the *lacO* array together with a TdTomato-tagged test construct that can only localize to the *lacO* array if it binds to the bait protein. Colocalization of GFP and TdTomato to the *lacO* array indicates molecular interaction between the two proteins (Figure 4A). When wild-type CENP-L or CENP-N were targeted to the *lacO* array, we observed that the reciprocal protein was recruited to the *lacO* array (CENP-N or CENP-L, respectively; Figure 4, B–D), but not other CCAN proteins (Supplemental Figure 4, A and B). The absence of other CCAN proteins is consistent with the complex interdependencies that exist within the CCAN that additionally rely on the presence of CENP-A and CENP-C (McKinley *et al.*, 2015; Weir *et al.*, 2016; Pesenti *et al.*, 2018). Therefore, this *lacO* array assay allows us to test the how mutating the CDK phosphorylation sites affects the interaction between CENP-L and CENP-N. Preventing CENP-L or CENP-N phosphorylation using phosphonull mutants altered their interactions in this *lacO* tethering assay only modestly (Figure 4, B–D). In contrast, phosphomimetic versions of either CENP-N or CENP-L were unable to recruit the reciprocal protein (Figure 4, B–D). We conclude that mimicking constitutive phosphorylation of either CENP-N or CENP-L is sufficient to prevent the interaction between these two proteins.

in the inducible knockout (iKO) cell line. Each dot in the graph represents the percentage of cells of cells with mitotic defects counted in three separate experiments. In each experiment at least 100 mitotic cells were randomly assessed for mitotic defects using microtubule stain to identify cells in mitosis (not shown). Multiple clones for each cell line were assessed to similar results—data shown were collected from a single clone over three experiments. The control sgRNA used is a guide that cuts at a single time in the genome (van den Berg *et al.*, 2018). Error bars represent standard deviations. Unpaired two-tailed *t* test was performed. *p* values from left to right:*** = 0.0009, *** = 0.0007, ** = 0.0071, ns = 0.5652.

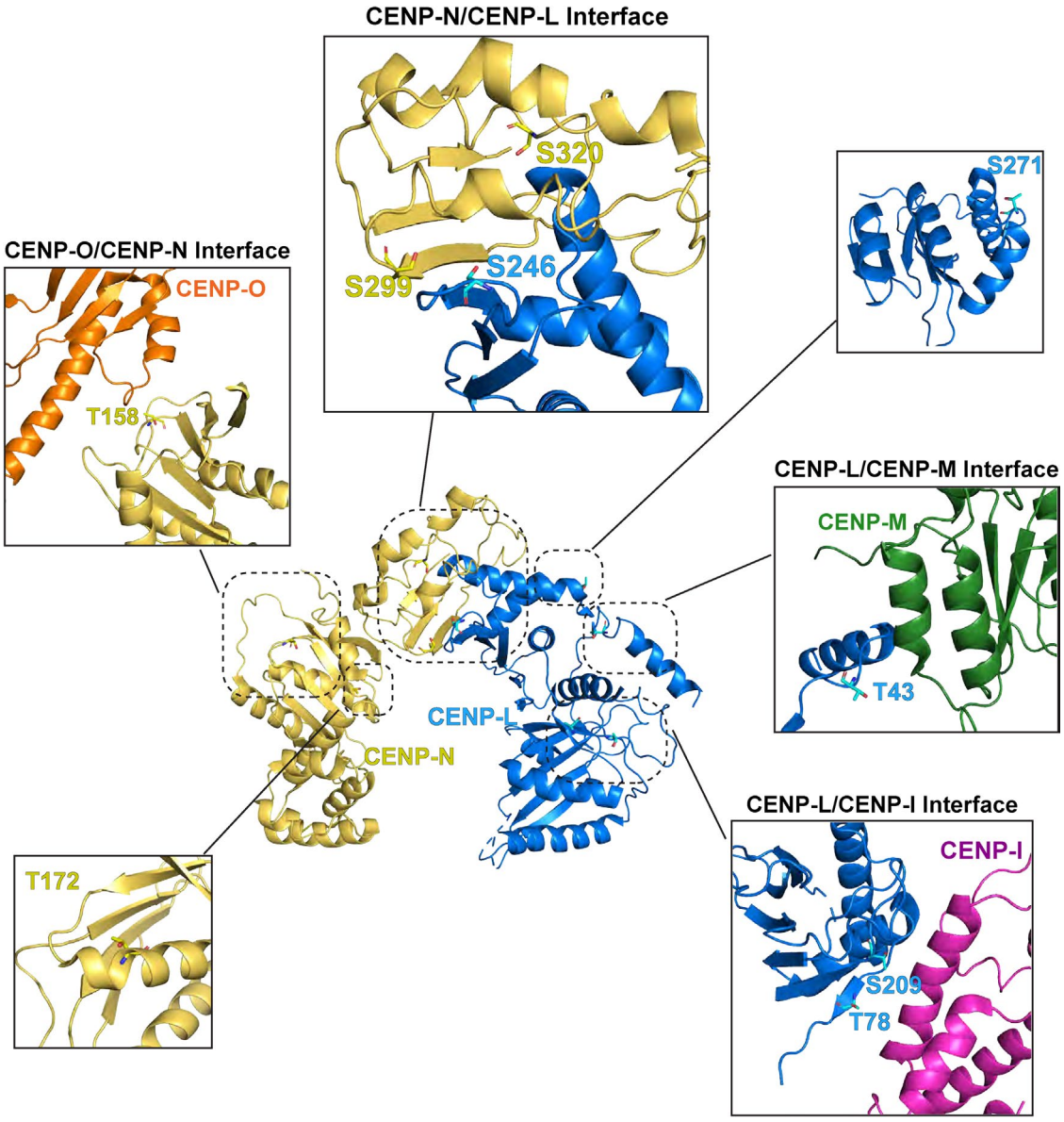

FIGURE 3: CDK sites in CENP-L and CENP-N are located at interaction interfaces between each protein and other proteins of the CCAN. Cartoon model of CENP-L (shown in blue) and CENP-N (shown in yellow) adapted from PDB:7QOO (Pesenti *et al.*, 2022) with amino acid residues of interest represented as sticks. *Note:* The following residues are not present in the structure: CENP-N: T220; CENP-L: T10, T25. Only a portion of the structure is represented in this figure. Each boxed region highlights where each amino acid residue is in the CENP-L/N structure and the interaction interface that is represented in the larger CCAN structure not included in this simplified figure. The following amino acid residues are shown for each interacting protein: CENP-O (shown in orange):110–203; CENP-M (shown in green): 65–130; CENP-I (shown in magenta): 334–662.

Phosphorylation of the CENP-N N-terminus disrupts its localization to kinetochores

We next sought to dissect the effects that mutating the CDK consensus residues has on the established functional domains for CENP-N. The association of CENP-N with kinetochores is dependent on its direct interaction with CENP-A (Carroll *et al.*, 2010; McKinley *et al.*, 2015). Structure–function analysis has defined the N-terminal region of CENP-N (aa 1-212) as both necessary and sufficient for its localization to the kinetochore during interphase and its interaction with CENP-A (Supplemental Figure 5A; Carroll *et al.*, 2009; Pentakota *et al.*, 2017; Chittori *et al.*, 2018; Tian *et al.*, 2018; Allu *et al.*, 2019). Recent structural studies have also suggested that the localization of CENP-N to kinetochores utilizes additional interactions with centromeric DNA through a channel formed with CENP-L, as well as interactions with other CCAN proteins such as the CENP-O complex (Pesenti *et al.*, 2022; Yatskevich *et al.*, 2022). In the structure of CENP-N, two CDK consensus residues are present within the N-terminal region of CENP-N (T158 and T172) that form the interaction with CENP-O and participate in the DNA channel formed by CENP-N and CENP-L (Figure 3). To test whether mimicking constitutive phosphorylation of these two N-terminal residues affects the localization of CENP-N to kinetochores, we mutated these residues in an N-terminal fragment (CENP-N$^{1\text{-}212}$). Although the wild-type N-terminal CENP-N fragment (CENP-N$^{1\text{-}212}$) localized to kinetochores during interphase, a similar construct mimicking constitutive phosphorylation for the CDK consensus sites was unable to localize to kinetochores

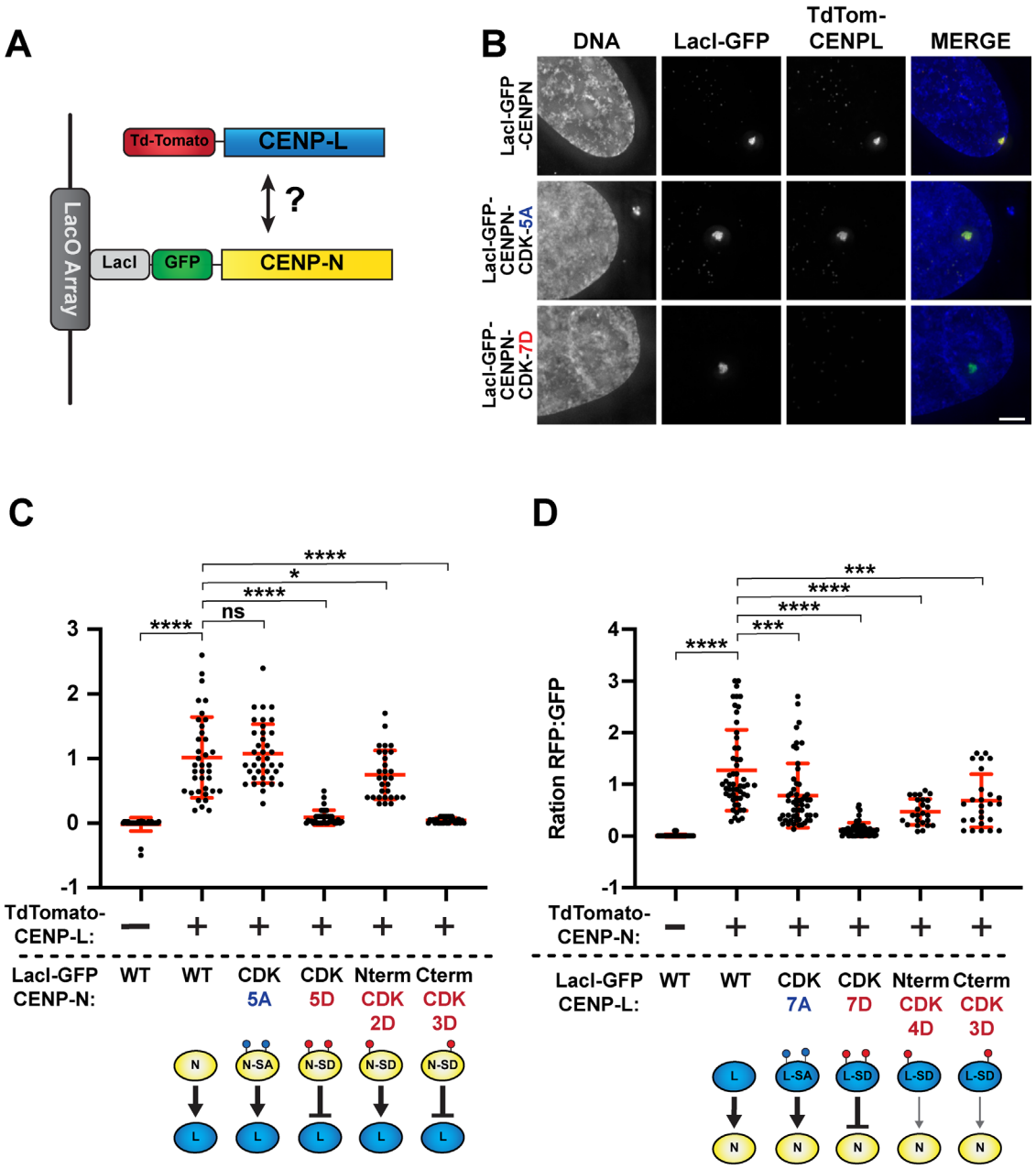

FIGURE 4: Phosphorylation state affects the interaction between CENP-N and CENP-L. (A) Diagram illustrating the *lacO* ectopic targeting assay. (B) Representative images of the Lac array assay for LacI-GFP-CENP-N mutants and the recruitment of TdTomato-CENP-L. GFP and TdTomato images are scaled the same. Images are max projected and deconvolved. Scale bar is 5 μm. (C, D) Quantification of fluorescence intensity for recruitment of TdTomato-tagged constructs to the *lacO* array by the LacI-GFP bait protein. Each dot represents the ratio between RFP:GFP fluorescence at a single focus. Data were collected from three separate experiments. Error bars represent SD. Unpaired two-tailed *t* test was performed. For C, *p* values presented for brackets going from left to right: **** = < 0.0001, ns = 0.6305, **** = < 0.0001, * = 0.0429, **** = < 0.0001. N values from left to right: *N* = 38, *N* = 37, *N* = 38, *N* = 38, *N* = 30, *N* = 30. For D, *p* values presented for brackets from left to right: **** = < 0.0001, *** = 0.005, ****< 0.001, *** = 0.008. *N* values from left to right: 41, 53, 53, 54, 54, 25, 26.

(Supplemental Figure 5A). Similarly, a full-length CENP-N construct with phosphomimetic versions of only the N-terminal residues (T158D, T172D; referred to as CENP-N$^{NtermCDK\text{-}2D}$; Figure 5A) was also unable to localize to kinetochores at any cell cycle stage (Figure 5A) and was unable to rescue proper chromosome segregation in the absence of the endogenous protein (Figure 5, B and C). Together, this suggests that the CDK consensus sites present within the N-terminus of CENP-N regulate the kinetochore localization of CENP-N.

Phosphorylation of the CENP-N C-terminus regulates CENP-N-CENP-L interactions

The C-terminus of CENP-N is necessary to mediate its interaction with CENP-L and is required to facilitate CENP-N's kinetochore localization during mitosis (Carroll *et al.*, 2009; Hinshaw and Harrison, 2013; McKinley *et al.*, 2015; Pentakota *et al.*, 2017). Indeed, the CDK consensus sites present within the C-terminus of CENP-N lie directly within the interface between CENP-N and CENP-L

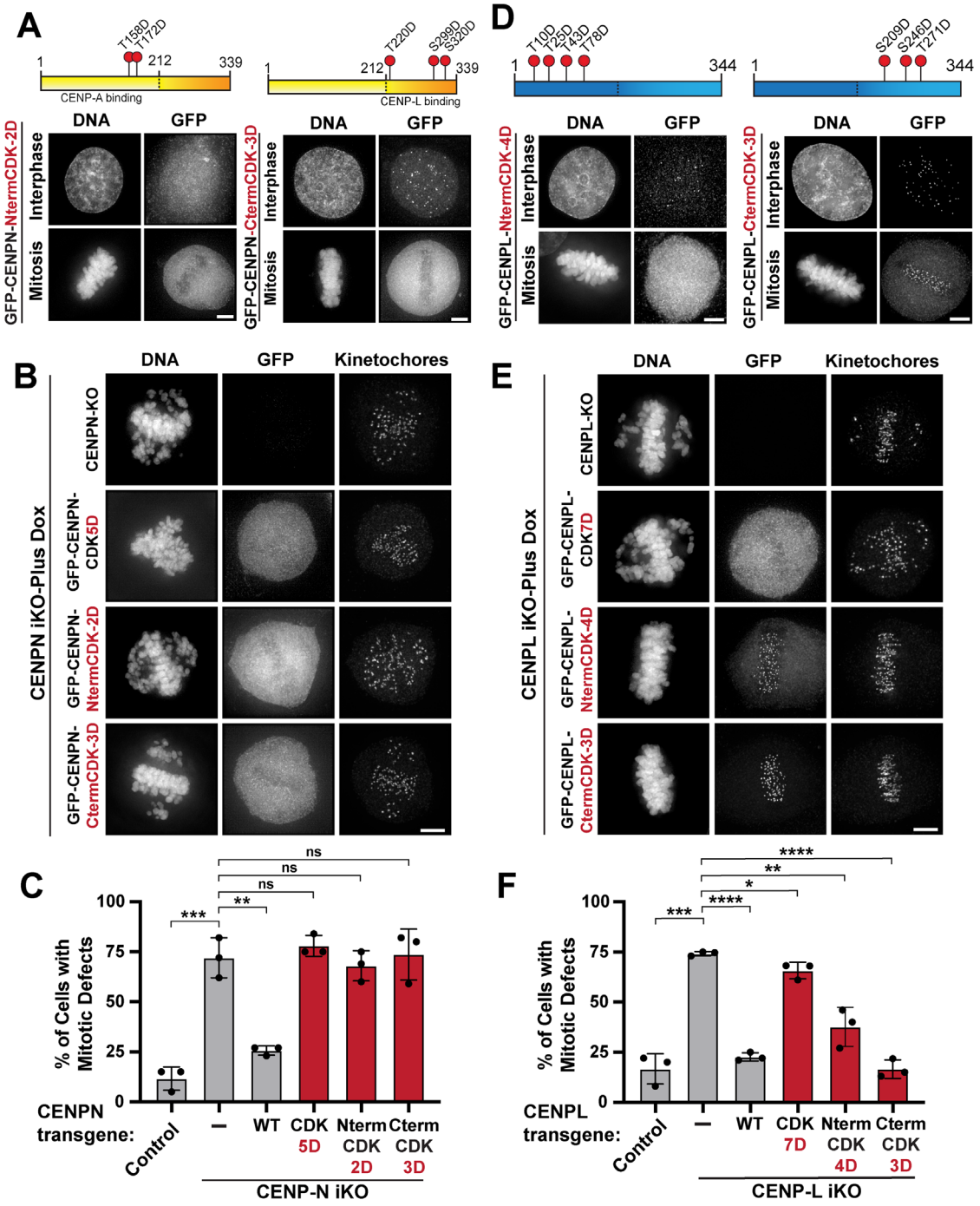

FIGURE 5: Splitting phosphomimetic point mutations between the N and C terminus results in differential localization behavior. (A) Representative images of mitotic and interphase cells demonstrating the localization of CENP-N split phosphomutants stably expressed in HeLa cells in the presence of endogenous protein. Showing DNA (Hoechst) and GFP (GFP booster). Diagrams illustrate what sites were mutated in each GFP-tagged construct. Images are deconvolved and max projected. Scale bar is 5 μm. (B) Representative images of mitotic phenotypes from CENP-N inducible knockout cell lines expressing the indicated GFP-tagged guide-resistant constructs after 5-day induction of CENP-N knockout. Shown in the figure is DNA (Hoechst), GFP, Kinetochores (anti-centromere antibodies (ACA). Images are deconvolved and max projected. Scale bar is 5 μm. (C) Quantification of mitotic cells with defects observed in GFP-CENPN replacement cell lines following inducible knockout (iKO) of endogenous CENP-N for 5 d. Mitotic defects include misaligned chromosomes and multipolar spindles. Each dot in the graph represents the percentage of cells with mitotic defects counted in three separate experiments. In each experiment at least 100 mitotic cells were randomly assessed for mitotic defects using microtubule stain to identify cells in mitosis (not shown). Multiple clones for each cell line were assessed to similar results; data shown were collected from a single clone over three separate experiments. The control sgRNA used is a guide that cuts at a single time in the genome (van den Berg *et al.*, 2018). Error bars represent standard deviations. Unpaired two-tailed *t* test was performed. *p* values from left to right: *** = 0.0008,

(Figure 3). To test how phosphorylation affects the CENP-N-CENP-L interaction, we generated phosphomimetic mutants that specifically target the residues in the CENP-N C terminus (CENP-N$^{CtermCDK\text{-}3D}$: T220D, S299D, S320D; Figure 5A). The CENP-N$^{CtermCDK\text{-}3D}$ mutant displayed differential cell cycle–dependent localization to kinetochores. Although the CENP-N$^{CtermCDK\text{-}3D}$ mutant maintained its ability to localize to kinetochores during interphase, this mutant did not localize to kinetochores in mitosis. This altered temporal localization recapitulates the localization behavior of truncating the CENP-N C-terminus (Δ212-339), supporting the functional requirement of the C-terminal region of CENP-N in maintaining its kinetochore localization in mitosis (Supplemental Figure 5B). Consistent with this localization behavior, this mutant failed to restore mitotic function in the absence of endogenous CENP-N (Figure 5, B and C) and failed to associate with CENP-L in the *lacO* tethering assay (Figure 4C). Together, these observations suggest that the CDK consensus sites present within the CENP-N C-terminus regulate the interaction between CENP-L and CENP-N, an interaction that is essential for the constitutive localization of the CENP-L/N complex throughout the cell cycle.

Phosphorylation sites in both the CENP-L N-terminus and C-terminus regulate its localization behavior

CENP-L interacts with both CENP-N and other CCAN components. However, until the publication of the recent structural studies (Pesenti *et al.*, 2022; Yatskevich *et al.*, 2022), the functional domains of human CENP-L protein were less clearly defined. Structural predictions for CENP-L and comparisons to the structure of the yeast CENP-L ortholog suggested that the N-terminus of CENP-L has structural homology to CENP-N, whereas the C-terminus mediates its interaction with CENP-N (Hinshaw and Harrison, 2013; Pentakota *et al.*, 2017). To test the functional contributions of each domain of CENP-L, we generated phosphomimetic mutants targeting the CDK sites in either the N- or C-terminal regions of CENP-L. Given the distribution of the phosphorylation sites within the protein and secondary structure predictions, we defined the N-terminal domain of CENP-L as amino acids 1–172 (CENP-L$^{NtermCDK\text{-}4D}$) and the C-terminal region as amino acids 173–344 (CENP-L$^{CtermCDK\text{-}3D}$) (Figure 5D). Interestingly, the two split phosphomimetic mutants displayed distinct localization behavior. In the presence of endogenous CENP-L, the CENP-L$^{NtermCDK\text{-}4D}$ mutant displayed reduced localization to kinetochores during interphase and failed to localize in mitosis (Figure 5D). This suggests that the CENP-L$^{NtermCDK\text{-}4D}$ mutant cannot compete against the endogenous protein for localization to the kinetochore in mitosis. Consistent with this altered localization, the CENP-L$^{NtermCDK\text{-}4D}$ mutant showed reduced recruitment of CENP-N in the *lacO*/LacI assay, although this mutant was less defective than the full CENP-L$^{CDK\text{-}7D}$ mutant (Figure 4D). However, kinetochore localization of the CENP-L$^{NtermCDK\text{-}4D}$ mutant was restored in both interphase and mitosis following depletion of the endogenous protein (Figure 5E) and was able largely to rescue chromosome segregation defects (Figure 5F). In contrast, the CENP-L$^{CtermCDK\text{-}3D}$ mutant was functional for its ability to localize and rescue mitotic phenotypes in the replacement cell line (Figure 5, D–F). Additionally, the CENP-L$^{CtermCDK\text{-}3D}$ mutant recruited CENP-N to the *lacO* array in the *lacO*/LacI-binding assay better than the CENP-L$^{CDK\text{-}7D}$ and the CENP-L$^{NtermCDK\text{-}4D}$ mutants (Figure 4D), although none of these mutants recruited CENP-N as well as the wild-type protein. Given that both CENP-L split mutants can interact with CENP-N to different degrees, this suggests that both the N-terminus and C-terminus of CENP-L contribute to its kinetochore localization. This is reinforced by the recent structures of human CENP-L, which demonstrates that residues from both the N- and C- terminus of CENP-L contribute to its interaction with CENP-N and other proteins of CCAN such as CENP-I and CENP-M (Pesenti *et al.*, 2022; Yatskevich *et al.*, 2022). Therefore, disrupting a single interaction interface is not sufficient to completely delocalize CENP-L from kinetochores.

Disrupting phosphorylation prevents CENP-LN complex kinetochore targeting

The results described above suggest that mimicking constitutive phosphorylation of either CENP-L or CENP-N is sufficient to disrupt CENP-LN complex interactions and kinetochore localization. In contrast, preventing the phosphorylation of either protein did not result in significant defects in CENP-LN complex formation or function. One possible explanation for this discrepancy is that phosphorylation of one subunit of this complex is sufficient to regulate the CENP-L-CENP-N interaction. Indeed, phosphomimetic CENP-L$^{CDK\text{-}7D}$ mutants are unable to interact with either wild-type CENP-N or the CENP-N$^{CDK\text{-}5A}$ mutants in the *lacO* ectopic targeting assay (Supplemental Figure 6A). Therefore, to assess the consequences of failing to regulate the CENP-LN complex downstream of CDK, we hypothesized that it would be necessary to prevent the phosphorylation of both CENP-N and CENP-L simultaneously. Despite repeated attempts, we were unable to isolate cell lines stably coexpressing CENP-N$^{CDK\text{-}5A}$ and CENP-L$^{CDK\text{-}7A}$ (unpublished data). Thus, to

** = 0.0014, ns = 0.4086, ns = 0.6098, ns = 0.8672. I GFP-CENP-N$^{NtermCDK\text{-}2D}$ replacement cell line is not a clonal cell line, and is only enriched for GFP fluorescence. All other GFP rescue cell lines are clonal. (D) Representative images of mitotic and interphase cells demonstrating the localization of CENP-L split phosphomutants stably expressed in HeLa cells in the presence of endogenous protein. DNA (Hoechst) and GFP (GFP booster) are shown. Diagrams illustrate what sites were mutated in each GFP-tagged construct. Images are deconvolved and max projected. Scale bar is 5 μm. (E) Representative images of mitotic phenotypes from CENP-L inducible knockout cell lines expressing the indicated GFP-tagged guide-resistant constructs after 5-day induction of CENP-L knockout. Shown in the figure are DNA (Hoechst), GFP, and kinetochores (anti-centromere antibodies [ACA]). Images are deconvolved and max projected. Scale bar is 5 μm. (F) Quantification of mitotic cells with defects observed in GFP-CENP-L replacement cell lines following inducible knockout (iKO) of endogenous CENP-L for 5 d. Mitotic defects include misaligned chromosomes and multipolar spindles. Each dot in the graph represents the percentage of cells with mitotic defects counted in three separate experiments. In each experiment at least 100 mitotic cells were randomly assessed for mitotic defects using microtubule stain to identify cells in mitosis (not shown). Multiple clones for each cell line were assessed to similar results-data shown was collected from a single clone over three experiments. The control sgRNA used is a guide that cuts at a single time in the genome (van den Berg *et al.*, 2018). Error bars represent standard deviations. Unpaired two-tailed *t* test was performed. *p* values from left to right: *** = 0.0002, **** = < 0.0001, * = 0.0255, ** = 0.0029, **** = < 0.0001.

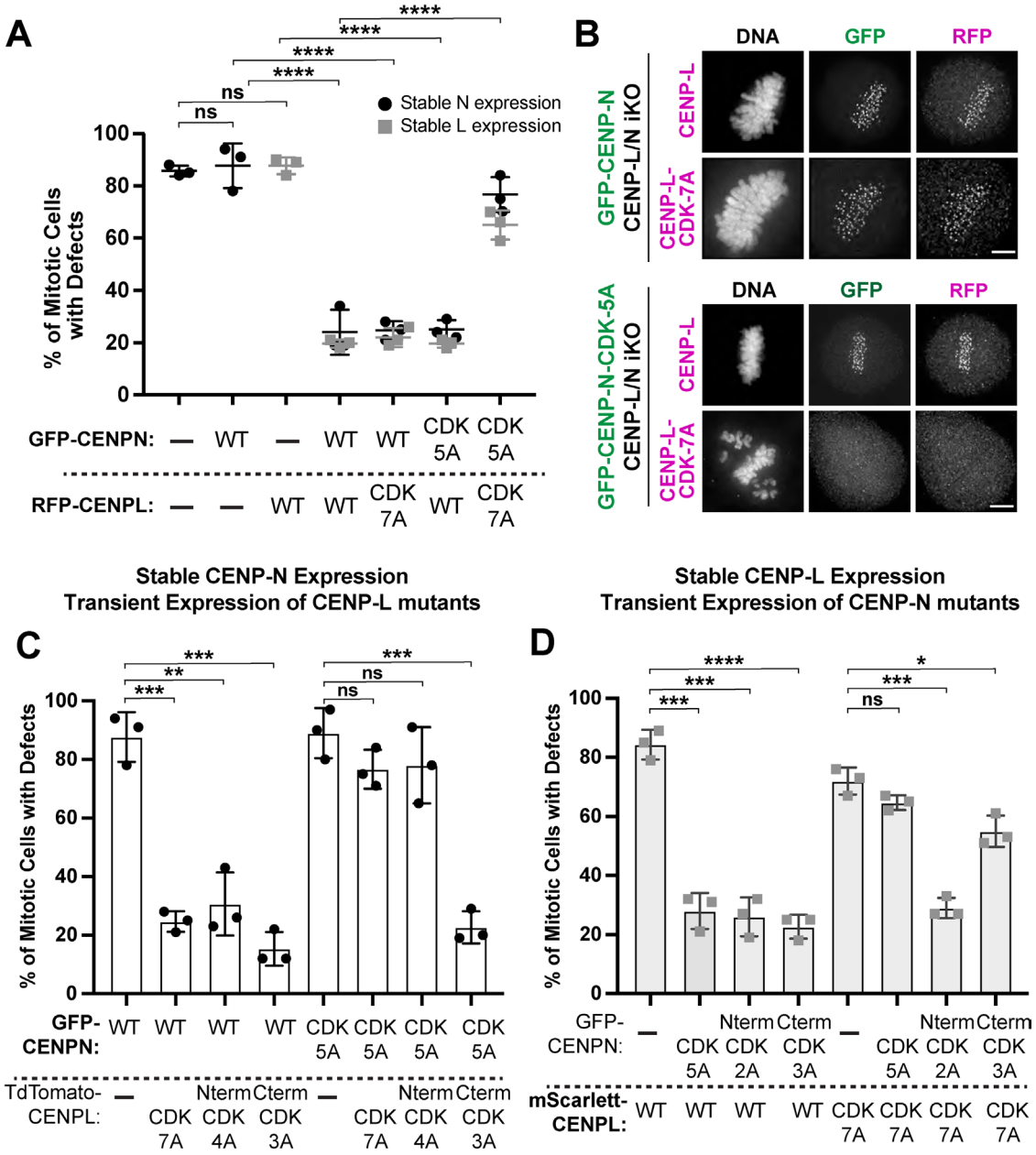

FIGURE 6: Preventing phosphorylation of both proteins negatively affects the function of the CENP-LN complex. (A) Quantification of mitotic cells with defects observed in CENP-L/CENP-N dual inducible knockout (iKO) cell lines following 5 d of knockout of endogenous. In the stable N expression experiments (represented by black dots), Td-Tomato-tagged CENP-L constructs were transiently transfected on the third day of dox induction, 48 h before cells were fixed. The inverse was done for the stable L expression (represented by gray dots) experiments. Each dot represents the percent of cells with mitotic defects counted in three separate experiments. Approximately 75 cells were counted per condition; cells were selected by finding cells expressing a control plasmid expressing a GFP or RFP alone (not shown). Multiple clones for each cell line were assessed with similar results—data shown were collected from a single clone over three experiments. Unpaired two-tailed *t* test was performed. *p* values from left to right: ns = 0.7126, ns = 0.4169, all **** = <0.0001. (B) Representative immunofluorescence images of mitotic phenotypes from CENP-L/N inducible knockout cell lines stably expressing either GFP-CENPN or CENP-CENPN$^{CDK\text{-}5A}$ and transiently expressing TdTomato-tagged CENP-L or CENP-L$^{CDK\text{-}7A}$ constructs 48 h before fixing. Images are deconvolved and max projected. Scale bar is 5 µm. (C) Quantification of mitotic cells with defects observed in CENP-L/CENP-N dual inducible knockout (iKO) cell lines following 5 d of knockout of endogenous stably expressing either GFP-CENP-N or GFP-CENP-N$^{CDK\text{-}5A}$ and transiently expressing TdTomato-CENP-L constructs for 48 h before fixation. Each dot represents the percent of cells with mitotic defects counted in three separate experiments. Approximately 75 cells were counted per condition; cells were selected by finding cells expressing a control plasmid expressing a GFP or RFP alone (not shown). Multiple clones for each cell line were assessed with similar results—data shown were collected from a single clone over three experiments. Unpaired two-tailed *t* test was performed. *p* values from left to right: *** = 0.0003, ** = 0.0020, *** = 0.0003, ns = 0.1199, ns = 0.2879, *** = 0.0003. (D) Quantification of mitotic cells with defects observed in CENP-L/

circumvent potential technical challenges associated with expressing both mutants constitutively, we developed a conditional strategy. For these experiments, we stably expressed either CENP-N$^{CDK\text{-}5A}$ or CENP-L$^{CDK\text{-}7A}$ individually in a double inducible knockout cell line expressing guides targeting both CENP-N and CENP-L simultaneously. Following 3 d of Cas9 induction to deplete the endogenous protein, we then transiently expressed the reciprocal binding partner and assessed kinetochore localization and mitotic phenotypes 48 h after transfection (5 d total of CENP-L/N depletion).

In cell lines stably expressing either GFP-CENP-N or the GFP-CENP-N$^{CDK\text{-}5A}$ mutant, transient transfection of wild-type TdTomato-CENP-L restored localization of both GFP-CENP-N and GFP-CENP-N$^{CDK\text{-}5A}$ (Figure 6, A and B, black data points). Similarly, transiently expressing the TdTomato-CENPL$^{CDK\text{-}7A}$ mutant restored localization and rescued mitotic function in cell lines stably expressing the wild type GFP-CENP-N. In contrast, combining the TdTomato-CENPL$^{CDK\text{-}7A}$ and GFP-CENP-N$^{CDK\text{-}5A}$ mutants resulted in the failure of either protein to localize to kinetochores and severe mitotic defects (Figure 6, A and B). We observed similar results in experiments using cell lines stably expressing either CENP-L or the CENP-L$^{CDK\text{-}7A}$ mutant with the transient introduction of CENP-N constructs (Figure 6A, gray data points). Importantly, although combining the CENP-N$^{CDK\text{-}5A}$ and CENP-L$^{CDK\text{-}7A}$ mutants in the replacement assay prevented kinetochore localization, these mutants were able to interact with each other in our *lacO* ectopic targeting assay, although modestly reduced relative to the wild-type proteins (Supplemental Figure 6B). This suggests that the absence of proper kinetochore localization is due to a defect in the loading or recruitment of the CENP-N$^{CDK\text{-}5A}$/CENP-L$^{CDK\text{-}7A}$ complex to kinetochores.

Finally, to dissect the minimal requirements for this synergistic defect in the absence of CDK phosphorylation, we tested split phosphonull mutants to target a subset of phosphorylation sites in each protein (Figure 5, A and D). In our dual replacement assay, the split mutants for both CENP-L and CENP-N showed different behavior. We found that preventing phosphorylation of the CENP-L N-terminus (CENP-L$^{NtermCDK\text{-}4A}$) failed to rescue localization and mitotic function in cell lines stably expressing CENP-N$^{CDK\text{-}5A}$ (Figure 6C). In contrast, the CENP-L$^{CtermCDK\text{-}3A}$ mutant fully rescued mitotic function and localization of the CENP-N$^{CDK\text{-}5A}$ mutant (Figure 6D). Additionally, we found that the C-terminal CENP-N$^{CtermCDK\text{-}3A}$ phosphomutant failed to rescue mitotic function in cells stably expressing CENP-L$^{CDK\text{-}7A}$ mutant, but that the CENP-N$^{NtermCDK\text{-}2A}$ mutant restored mitotic function and localization of both mutants in these cells (Figure 6D). Therefore, preventing phosphorylation specifically of the C-terminus of CENP-N, which mediates the interaction with CENP-L, and the N-terminus of CENP-L, which mediates interactions with other CCAN proteins, result in mitotic failure when their interacting partners are also not phosphorylated. This suggests that the C-terminus of CENP-N plays a critical role in regulating its interaction with CENP-L, and that the regulation of this interaction is important for dynamic CENP-L/N complex localization throughout the cell cycle.

Cycles of dynamic phosphorylation drive inner kinetochore reorganization

Together, our data support a model in which dynamic cycles of phosphorylation act to regulate the recruitment of CENP-L and CENP-N to kinetochores in a cell cycle–dependent manner. Current structural models propose that there are sub stoichiometric amounts of CENP-N associated with centromere chromatin during mitosis (Allu *et al.*, 2019), but the basis for this change was unclear. To explain this behavior, prior studies suggested that the association of CENP-N with kinetochores is determined by the CENP-A chromatin state (Carroll *et al.*, 2009; Fang *et al.*, 2015; Allu *et al.*, 2019). Indeed, CENP-N has been shown to have lower affinity for compact CENP-A chromatin in vitro (Fang *et al.*, 2015). However, this model does not consider the functional importance of the interaction between CENP-N and CENP-L, and more broadly their interaction with other CCAN proteins at kinetochores throughout the cell cycle. Additionally, recently published structures of the human kinetochore have provided an alternative model for how the assembled CCAN associates with centromere chromatin (Pesenti *et al.*, 2022; Yatskevich *et al.*, 2022). In this new model, the CCAN not only interacts with CENP-A nucleosomes, but also associates with centromere DNA through a channel formed by CENP-L and CENP-N. The formation of this CENP-L/N-DNA channel is thought to be established through the interactions the CENP-L/N complex makes with other protein complexes of the CCAN. This new model for CCAN assembly at the centromere highlights the important role the CENP-LN complex plays in directing the assembly of the CCAN at the centromere.

Our work demonstrates that the interactions made by the CENP-LN complex within the CCAN can be regulated in a cell cycle–dependent manner due to the presence of the CDK consensus phosphorylation sites at these critical interaction interfaces. We find that phosphorylation of CENP-N at the CDK sites identified in our study has the potential to disrupt the interactions required for its initial kinetochore localization and its interaction with CENP-L, which is needed to maintain CENP-N at the kinetochore in mitosis. Additionally, the CDK-consensus sites identified in CENP-L are also present at critical interaction interfaces with CENP-HIKM and CENP-N, which can function to alter the localization behavior of CENP-L and therefore the CENP-LN complex. We propose a model in which phosphorylation of the CENP-LN complex can contribute to changes in the kinetochore localization and levels of this complex throughout the cell cycle. First, as cells progress through G2 and into mitosis, phosphorylation of a subset of CENP-L/N complex molecules in the cell (based on the imperfect CDK consensus for many of these sites) would result in a decrease in the total amount of CENP-L/N molecules at kinetochores, essentially acting as a molecular "pruning" event. Dephosphorylation of both CENP-L and CENP-N is then required following exit from mitosis to enable their interaction and loading onto the centromere (Figure 7). These dynamic cycles of phosphorylation and dephosphorylation are critical for proper CENP-LN localization, as simultaneously

CENP-N dual inducible (iKO) knockout cell lines following 5 d of knockout of endogenous stably expressing either mScarlett-CENP-L or mScarlett-CENP-L$^{CDK\text{-}7A}$ and transiently expressing GFP-CENP-N constructs for 48 h before fixation. Each dot represents the percent of cells with mitotic defects counted in three separate experiments. Approximately 75 cells were counted per condition; cells were selected by finding cells expressing a control plasmid expressing a GFP or RFP alone (not shown). Multiple clones for each cell line were assessed with similar results—data shown were collected from a single clone over three experiments. Unpaired two-tailed *t* test was performed. *p* values from left to right: *** = 0.0002, *** = 0.0003, ****–< 0.0001, ns = 0.0720, *** = 0.0002, * = 0.0136.

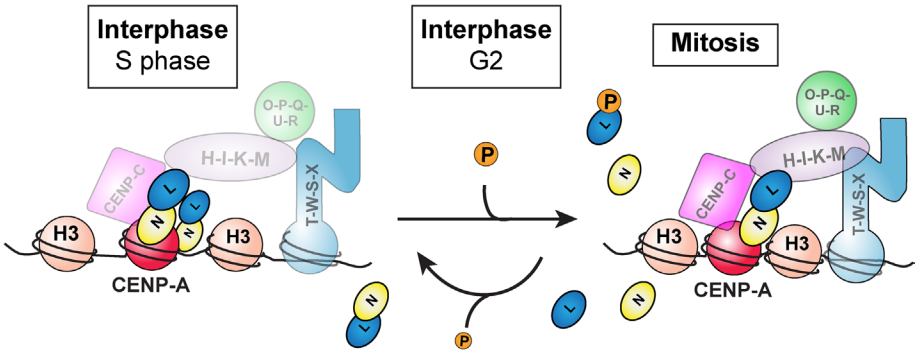

FIGURE 7: Modulating the interaction between CENP-L and CENP-N impacts the localization behavior of the CENP-L/N complex throughout the cell cycle. Phosphorylation functions to weaken the interaction between CENP-L and CENP-N. Based on our data, the CENP-LN complex is phosphorylated upon entry into mitosis. This phosphorylation event functions to break the interaction between a subset of CENP-N and CENP-L molecules resulting in their dissociation from the centromere. Following phosphorylation in mitosis, CENP-L and CENP-N must then be dephosphorylated to relocalize them to the centromere during S-phase.

preventing phosphorylation of CENP-L and CENP-N also negatively affects the behavior of this complex in the cell. Thus, despite the constitutive presence of the CENP-LN complex at centromeres, this dynamic regulatory control allows the inner kinetochore to set different organization and assembly states throughout the cell cycle.

METHODS

All reagents are available upon request.

Request a protocol through *Bio-protocol*.

Molecular biology

The CENP-L targeting sgRNA (TCTGCAGAAACGATTAGAAT) was cloned into pLenti-sgRNA with either puro resistance or blast resistance. The CENP-N inducible knockout cell line was published previously in McKinley *et al.* (2015). The gRNA used in our control was published in van den Berg *et al.* (2018) and cuts a single time in chromosome one (sgRNA sequence: GCCGATGGTGAAGTGGTAAG). All GFP-tagged constructs used for expression in replacement cell lines were generated by cloning codon-optimized guide-hardened human cDNA into a pBABE-blast vector (pIC242) containing an N-terminal LAP tag (GFP-TEV-S) as described in Cheeseman and Desai (2005). For single-replacement cell lines, the constructs used were (plasmid(p)/Cell line (c)): GFP-CENP-N (pKM619/cKM154); GFP-CENP-N^{CDK5A} (pAN2/cAN1); GFP-CENP-N^{CDK5D} (pAN14/cAN10); GFP-CENP-N$^{NtermCDK-2D}$ (pAN435/cAN182); GFP-CENP-N$^{NtermCDK-2A}$ (pAN434/cAN181); GFP-CENP-N$^{CtermCDK-3A}$ (pAN436/cAN183); GFP-CENP-N$^{CtermCDK-3D}$ (pAN437/cAN184); GFP-CENP-L (pAN200/cAN81); GFP-CENP-L^{CDK7A} (pAN233/cAN81); GFP-CENP-L^{CDK7D} (pAN234/cAN83); GFP-CENP-L$^{NtermCDK-4D}$ (pAN238/cAN94); GFP-CENP-L$^{NtermCDK-4A}$ (pAN235/cAN91); GFP-CENP-L$^{CtermCDK-3A}$ (pAN236/cAN92); GFP-CENP-L$^{CtermCDK-3D}$ (pAN237/cAN93). The CENP-N and CENP-L split mutants were constructed by two rounds of overlap PCR using both the wild type and mutant cDNA's. Dual-replacement CENP-N and CENP-L expressing transgene was generated by synthesizing a mEGFP-MCS-T2A-mScarlett-MCS gene fragment and cloning this into a pLenti vector under UbC promoter with a Hygromycin resistance cassette (pAN298). CENP-L and CENP-N sequences hardened to the guides were then cloned into this plasmid. All plasmids were sequenced and verified by Genewiz Sanger Sequencing.

Cell culture conditions

HeLa cell lines were cultured in DMEM supplemented with 10% fetal bovine serum (FBS), 100 U/mL penicillin/streptomycin, and 2 mM L-glutamine at 37°C with 5% CO_2. The inducible Cas9 HeLa parental cell lines (cTT20.11) were generated by transposon integration as described previously (McKinley *et al.*, 2015) and are neomycin-resistant. Inducible knockout cell lines were similarly cultured, except that the medium was supplemented with certified tetracycline-free FBS. Cell lines were monitored monthly for mycoplasma contamination. Inducible knockouts for CENP-L (cAN71) and CENP-N (cKM154) were created by introducing guides cloned into pLenti-sgRNA (puromycin-resistant; McKinley *et al.*, 2015) into the inducible Cas9 cell lines by lentiviral transduction (Wang *et al.*, 2015). Following lentiviral transduction, cells were then selected with 0.35 µg/mL puromycin for 10 d, changing media every 2–3 d. The CENP-L/CENP-N dual knockout cell line was generated by infecting the CENP-N knockout cell line with pLenti-Blast plasmid containing the CENP-L guide RNA (pAN156) as above. Cells were then selected for 2 weeks with 0.35 µg/mL puromycin and 2 µg/mL blasticidin for two weeks. The U2OS *lacO* array cell lines were previously reported in Gascoigne *et al.* (2011) cultured in media similar to those for Hela and maintained in 200 µg/mL hygromycin.

Clonal replacement cell lines expressing GFP-tagged fusions for CENP-N and CENP-L (plasmids listed above) were generated by retroviral transduction in the knockout cell line to each corresponding gene. Following retroviral infection, cells were selected with 2 mg/ml blasticidin (Life Technologies) for 2 weeks, changing media every 4 d. Cells were then FACS sorted for GFP expression into single clones. After 2 weeks of growth cells were screened for proper GFP expression. Dual-replacement cell lines were generated by introducing the dual-expression plasmids into the dual-knockout cell lines with lentivirus as before. Two days after infection cells were selected with 2 µg/ml blasticidin, 0.35 µg/mL puromycin, and 375 µg/mL hygromycin (Invitrogen) for approximately 14 d. Cells were then FACS sorted into single clones expressing both GFP and mScarlett. The following plasmids were introduced into the dual-knockout background to generate the dual-replacement cell line (plasmids [p]; Cell lines [c]): UbC-mEGFP-MCS-T2A-mScarlett-MCS-Hygro (pAN298/cAN137); UbC-mEGFP-CENPN-T2A-mScarlett-MCS-Hygro (pAN301/cAN138); UbC-mEGFP-MCS-T2A-mScarlett-CENPL-Hygro (pAN302/cAN139); UbC-mEGFP-CENPN-CDK5A-T2A-mScarlett-MCS-Hygro (pAN310/cAN160); UbC-mEGFP-MCS-T2A-mScarlett-CENP-L-CDK7A-Hygro (pAN311/cAN161); UbC-mEGFP-CENPN-T2A-mScarlett-CENPL-Hygro (pAN303/cAN140). Transient transfections were performed with Xtremegene-9 and Optimem as per manufacturer's instructions. Cells were transfected 24 h after seeding on poly-L-lysine–coated coverslips. Medium was changed on transfected cells 16 h posttransfection; cells were then fixed and processed for immunofluorescence 48 h posttransfection. Plasmids used for Lac Array Experiment: LacI-GFP-CENPN (pAN141); LacI-GFP-CENP^{CDK-5A} (pAN142); LacI-GFP-CENPN^{CDK-5D} (pAN143); LacI-GFP-CENPN$^{CDKNtern-2D}$ (pAN451); LacI-GFP-CENPN$^{CDKCterm-3D}$ (pAN453); TdTomato-CENP-L (pAN197); TdTomato-CENP-L^{CDK-7A} (pAN241); LacI-GFP-CENPL (pAN146); LacI-GFP-CENPL^{CDK-5D}

(pAN148); LacI-GFP- LacI-GFP-CENPL$^{CDKNterm\text{-}4D}$ (pAN216); LacI-GFP-CENPL$^{CDKCterm\text{-}3D}$ (pAN215); TdTomato-CENP-N (pAN149); TdTomato-CENPN^{CDK5D} (pAN150).

Replacement cell line generation

Replacement cell lines were generated using the inducible CRISPR Cas9 HeLa cell line generated previously as described in McKinley *et al.* (2015). The CENP-N knockout cell line was described previously in McKinley *et al.* (2015). The CENP-L knockout cell line was generated by introducing the CENP-L targeting guide into the inducible Cas9 cell line via lentiviral transduction as described in McKinley *et al.* (2015). Single-replacement cell lines were generated by introducing GFP-tagged constructs into their corresponding knockout cell lines by retroviral transfection followed by selection with 2 μg/mL blasticidin. Cells were then sorted for single clones. Where noted, cell lines enriched for fluorescence were not single-cell sorted but instead collected based on positive fluorescent signal. The CENP-LN dual-knockout cell line was generated by introducing the CENP-L guide cloned into a pLenti guide plasmid with blast resistance into the CENP-N ko cell line via lentiviral transduction. Cells were then selected with both 0.5 μg/ml puromycin and 2 μg/ml blasticidin for 2 wk. The dual-replacement transgene was also introduced via lentiviral transduction. Cells were then selected with 0.5 μg/ml puromycin, 2 μg/ml blasticidin, and 400 μg/mL hygromycin. Cells were then sorted for both single-cell clones and a fluorescently enriched population of cells.

To induce Cas9 mediation knockout of endogenous protein in the inducible knockout cell lines, cells were treated with 1 μg/mL doxycycline hyclate (Sigma) at 0 h, 24 h, and 48 h. Cells were then fixed and processed at 96 h (on day 5). For transfection into dual-replacement cell lines, cells were transfected on the third day of dox-induced Cas9 expression using Xtremegene (at the same time as addition of dox at 48 h postinduction). Media were changed 16 h posttransfection. Cells were fixed 48 h posttransfection.

Immunofluorescence and microscopy

Cells for immunofluorescence were seeded on glass coverslips coated with poly-L-lysine (Sigma-Aldrich). For all experiments, except those determining kinetochore levels throughout the cell cycle, cells were fixed in 4% formaldehyde (Sigma-Aldrich) diluted in PBS for 10 min. Coverslips were washed with PBS plus 0.1% Triton X-100 (PBS-TX). Blocking and primary antibody dilutions were performed in Abdil (20 mM Tris, 150 mM NaCl, 0.1% Triton X-100, 3% BSA and 0.1% NaN3, pH 7.5). GFP-booster (Chromotek; 1:500 dilution) was used to amplify GFP fluorescence for all experiments involving visualization of GFP-tagged transgenes. Kinetochores were detected using human anti-centromere antibody (ACA; Antibodies Inc #15234; 1:100 dilution). For assessment of mitotic phenotypes, microtubules were stained using DM1α (Sigma-Aldrich-F2168; 1:3000 dilution). For assessment of protein localization in the dual-replacement cell lines, the RFP signal was amplified with an anti-RFP antibody (Rockland-600-401-379; 1:3500 dilution). Cy2-, Cy3-, and Cy5-conjugated secondary antibodies (Jackson ImmunoResearch Laboratories) were used at a 1:300 dilution in PBS plus 0.1% Triton X-100. DNA was visualized by incubating cells in 1 μg/mL Hoechst33342 (Sigma-Aldrich) in PBS plus 0.1% Triton X-100 for 5 min. Coverslips were mounted using PPDM (0.5% p-phenylenediamine and 20 mM Tris-Cl, pH 8.8, in 90% glycerol) and sealed with nail polish. For cell cycle quantifications the following antibodies were used: anti-CENPC (1 μg/ml; Gascoigne *et al.*, 2011); anti-CENP-L (1:1500; McKinley *et al.*, 2015); anti-PCNA (Abcam-ab29; 1:500 dilution); anti-Cyclin B (Santa Cruz-sc245; 1:500 dilution); GFP-Booster (Chromotek; 1:500); anti-DM1α (Sigma-Aldrich-F2168; 1:3000) dilution; anti-ACA (Antibodies Inc #15234; 1:100 dilution). For GFP-tagged quantifications cells were fixed in 4% formaldehyde diluted in PBS and then treated with MeOH for 2 min at -20°C. For CENP-C quantification, cells were fixed in 4% formaldehyde diluted in PBSTx and then treated with MeOH for 2 min at -20°C. For CENP-L quantification, cells were preextracted for 7 min at room temperature using 0.5% PBSTx. G2 cells were identified using anti-CENP-F antibody (abcam-ab50; 1:500). Images were acquired on a DeltaVision Core deconvolution microscope (Applied Precision) equipped with a CoolSnap HQ2 charge-coupled device camera (Photometrics). For each image 40 Z-sections were acquired at 0.2 μm steps using a 100×, 1.4 NA Olympus U-PlanApo objective. All images were maximally projected and deconvolved as noted in the figure legends.

Quantification and statistical analysis

For quantification of fluorescence intensity, maximum-intensity projections were generated using the Deltavision Softworx Software (GE Healthcare). For image quantification, all images for comparison were acquired using the same acquisition settings. Integrated fluorescence intensity was measured using the MetaMorph software (Molecular Devices). For fluorescence intensity measurements at kinetochores, a 7 × 7–pixel region surrounding a kinetochore and a region in the surrounding area (background) were selected. Background measurements were subtracted from each kinetochore measurement. From 5 to 10 cells were imaged per cell cycle stage and at least 40 kinetochores were imaged per cell in each experiment (three total experiments). All values measured for kinetochores at G2 were divided by 2 because individual kinetochores cannot be resolved. Cells were randomly and blindly chosen based on the cell cycle marker. For each experiment, the average of all kinetochore fluorescence intensities was taken for cells and compared across cell cycle stages. The percentage of max fluorescence was then taken by comparing the fluorescence intensity of each cell cycle stage with the stage with the maximum fluorescence. For Lac array experiments, a 10 × 10 pixel regions surrounding a focus and a region in the surrounding area (background) were selected. Background measurements were subtracted from each focus measurement. Cells were randomly selected based on the presence of a LacI-GFP foci in the cell. For each cell the ratio of RFP:GFP fluorescence intensity was plotted to normalize intensity within each cell given the variability in expression that can result from transient transfection. For quantification of mitotic phenotypes in knockout and single-replacement cell lines, cells with mature metaphase spindle structures were evaluated. Cells with mitotic defects were defined as cells with multipolar spindles or at least one off-axis chromosome. At least 100 cells were quantified per condition in each experiment to ensure proper sampling of all cells on a given coverslip. For quantification of mitotic phenotypes in the dual replacement experiments, cells were selected based on both the presence of a mature mitotic spindle and expression of control plasmid expressing either RFP or GFP to ensure cell quantified was transfected. Due to limitations of transfection efficiency, at least 75 cells were quantified per condition. Statistical analyses were performed using Prism (GraphPad Software). Details of statistical analysis and sample sizes are provided in the figure legends.

Immunoprecipitation and mass spectrometry

For mitotically enriched immunoprecipitations, cells from 40 × 15–cm plates were arrested with 330 nM nocodazole (Sigma-Aldrich) for 16 h and harvested by shake-off. For cells enriched in

S-phase, cells from 40 × 15–cm plates were treated with 2 mM thymidine (Sigma-Aldrich) for 18 h and harvested with PBS plus 5 mM EDTA. Immunoprecipitations for mass spectrometry analysis were performed as described previously (Cheeseman and Desai, 2005). Harvested cells were washed in PBS and resuspended 1:1 in 1× Lysis Buffer (50 mM HEPES, 1 mM EGTA, 1 mM $MgCl_2$, 100 mM KCL, 10% glycerol, pH 7.4) and then drop frozen in liquid nitrogen. Cells were thawed after addition of an equal volume of 1.5× lysis buffer supplemented with 0.075% Nonidet P-40, 1× Complete EDTA-free protease inhibitor cocktail (Roche), 1 mM PMSF, 20 mM beta-glycerophosphate, 1 mM sodium fluoride, and 0.4 mM sodium orthovanadate. Cells were lysed by sonication and cleared by centrifugation. The supernatant was mixed with Protein A beads coupled to rabbit anti-GFP antibody (Cheeseman and Desai, 2005) and placed on a rotating wheel at 4°C for 1 h. Next, the beads were washed five times in 50 mM HEPES, 1 mM EGTA, 1 mM $MgCl_2$, 300 mM KCl, 10% glycerol, 0.05% NP-40, 1 mM DTT, 10 µg/ml leupeptin/pepstatin/chymostatin, pH 7.4 wash buffer (wash buffer). Following a final wash in wash buffer without detergent, bound protein was eluted with 100 mM glycine at pH 2.6. Eluted proteins were precipitated overnight by addition of 1/5 volume trichloroacetic acid at 4°C. Precipitated proteins were reduced with TCEP, alkylated with iodoacetamide, and digested with mass spectrometry grade Lys-C and trypsin (Promega). Digested peptides were purified using C18 spin columns (Pierce) according to the manufacturer's instructions. Samples were analyzed on an LTQ XL Ion Trap mass spectrometer (Thermo Fisher) coupled with a reverse phase gradient over C18 resin. Data were analyzed using Proteome Discoverer (Thermo Fisher).

ACKNOWLEDGMENTS

We thank the members of the Cheeseman lab for their suggestions and their contributions to this project. We would specifically like to thank Gunter Sissoko, Jimmy Ly, and Eric Smith for their time and guidance on experiments and data analysis in this work. This work was supported by grants from NIH/National Institute of General Medical Sciences (R35GM126930) and the NSF (2029868) to IMC and a National Science Foundation Graduate Research Fellowship to A.P.N.

REFERENCES

Allu PK, Dawicki-McKenna JM, Van Eeuwen T, Slavin M, Braitbard M, Xu C, Kalisman N, Murakami K, Black BE (2019). Structure of the human core centromeric nucleosome complex. Curr Biol 29, 2625–2639.e2625.

Amano M, Suzuki A, Hori T, Backer C, Okawa K, Cheeseman IM, Fukagawa T (2009). The CENP-S complex is essential for the stable assembly of outer kinetochore structure. J Cell Biol 186, 173–182.

Basilico F, Maffini S, Weir JR, Prumbaum D, Rojas AM, Zimniak T, De Antoni A, Jeganathan S, Voss B, van Gerwen S, *et al.* (2014). The pseudo GTPase CENP-M drives human kinetochore assembly. Elife 3, e02978.

Carroll CW, Milks KJ, Straight AF (2010). Dual recognition of CENP-A nucleosomes is required for centromere assembly. J Cell Biol 189, 1143–1155.

Carroll CW, Silva MC, Godek KM, Jansen LE, Straight AF (2009). Centromere assembly requires the direct recognition of CENP-A nucleosomes by CENP-N. Nat Cell Biol 11, 896–902.

Cheeseman IM (2014). The kinetochore. Cold Spring Harb Perspect Biol 6, a015826.

Cheeseman IM, Desai A (2005). A combined approach for the localization and tandem affinity purification of protein complexes from metazoans. Sci STKE 2005, pl1.

Cheeseman IM, Hori T, Fukagawa T, Desai A (2008). KNL1 and the CENP-H/I/K complex coordinately direct kinetochore assembly in vertebrates. Mol Biol Cell 19, 587–594.

Chittori S, Hong J, Saunders H, Feng H, Ghirlando R, Kelly AE, Bai Y, Subramaniam S (2018). Structural mechanisms of centromeric nucleosome recognition by the kinetochore protein CENP-N. Science 359, 339–343.

Earnshaw WC, Rothfield N (1985). Identification of a family of human centromere proteins using autoimmune sera from patients with scleroderma. Chromosoma 91, 313–321.

Falk SJ, Guo LY, Sekulic N, Smoak EM, Mani T, Logsdon GA, Gupta K, Jansen LE, Van Duyne GD, Vinogradov SA, *et al.* (2015). Chromosomes. CENP-C reshapes and stabilizes CENP-A nucleosomes at the centromere. Science 348, 699–703.

Fang J, Liu Y, Wei Y, Deng W, Yu Z, Huang L, Teng Y, Yao T, You Q, Ruan H, *et al.* (2015). Structural transitions of centromeric chromatin regulate the cell cycle–dependent recruitment of CENP-N. Genes Dev 29, 1058–1073.

Foltz DR, Jansen LE, Black BE, Bailey AO, Yates JR 3rd, Cleveland DW (2006). The human CENP-A centromeric nucleosome-associated complex. Nat Cell Biol 8, 458–469.

Gascoigne KE, Cheeseman IM (2013). CDK-dependent phosphorylation and nuclear exclusion coordinately control kinetochore assembly state. J Cell Biol 201, 23–32.

Gascoigne KE, Takeuchi K, Suzuki A, Hori T, Fukagawa T, Cheeseman IM (2011). Induced ectopic kinetochore assembly bypasses the requirement for CENP-A nucleosomes. Cell 145, 410–422.

Guo LY, Allu PK, Zandarashvili L, McKinley KL, Sekulic N, Dawicki-McKenna JM, Fachinetti D, Logsdon GA, Jamiolkowski RM, Cleveland DW, *et al.* (2017). Centromeres are maintained by fastening CENP-A to DNA and directing an arginine anchor-dependent nucleosome transition. Nat Commun 8, 15775.

Guse A, Carroll CW, Moree B, Fuller CJ, Straight AF (2011). In vitro centromere and kinetochore assembly on defined chromatin templates. Nature 477, 354–358.

Hara M, Fukagawa T (2020). Dynamics of kinetochore structure and its regulations during mitotic progression. Cell Mol Life Sci 77, 2981–2995.

Hellwig D, Emmerth S, Ulbricht T, Doring V, Hoischen C, Martin R, Samora CP, McAinsh AD, Carroll CW, Straight AF, *et al.* (2011). Dynamics of CENP-N kinetochore binding during the cell cycle. J Cell Sci 124, 3871–3883.

Hellwig D, Munch S, Orthaus S, Hoischen C, Hemmerich P, Diekmann S (2008). Live-cell imaging reveals sustained centromere binding of CENP-T via CENP-A and CENP-B. J Biophotonics 1, 245–254.

Hinshaw SM, Harrison SC (2013). An Iml3-Chl4 heterodimer links the core centromere to factors required for accurate chromosome segregation. Cell Rep 5, 29–36.

Hori T, Amano M, Suzuki A, Backer CB, Welburn JP, Dong Y, McEwen BF, Shang WH, Suzuki E, Okawa K, *et al.* (2008a). CCAN makes multiple contacts with centromeric DNA to provide distinct pathways to the outer kinetochore. Cell 135, 1039–1052.

Hori T, Okada M, Maenaka K, Fukagawa T. (2008b). CENP-O class proteins form a stable complex and are required for proper kinetochore function. Mol Biol Cell 19, 843–854.

Hornbeck PV, Zhang B, Murray B, Kornhauser JM, Latham V, Skrzypek E (2015). PhosphoSitePlus, 2014: mutations, PTMs and recalibrations. Nucleic Acids Res 43, D512–D520.

Huis In 't Veld PJ, Jeganathan S, Petrovic A, Singh P, John J, Krenn V, Weissmann F, Bange T, Musacchio A (2016). Molecular basis of outer kinetochore assembly on CENP-T. eLife 5, e21007.

Janicki SM, Tsukamoto T, Salghetti SE, Tansey WP, Sachidanandam R, Prasanth KV, Ried T, Shav-Tal Y, Bertrand E, Singer RH, Spector DL (2004). From silencing to gene expression: real-time analysis in single cells. Cell 116, 683–698.

Kato H, Jiang J, Zhou BR, Rozendaal M, Feng H, Ghirlando R, Xiao TS, Straight AF, Bai Y (2013). A conserved mechanism for centromeric nucleosome recognition by centromere protein CENP-C. Science 340, 1110–1113.

Kettenbach AN, Schweppe DK, Faherty BK, Pechenick D, Pletnev AA, Gerber SA (2011). Quantitative phosphoproteomics identifies substrates and functional modules of Aurora and Polo-like kinase activities in mitotic cells. Sci Signal 4, rs5.

Malvezzi F, Litos G, Schleiffer A, Heuck A, Mechtler K, Clausen T, Westermann S (2013). A structural basis for kinetochore recruitment of the Ndc80 complex via two distinct centromere receptors. EMBO J 32, 409–423.

McKinley KL, Sekulic N, Guo LY, Tsinman T, Black BE, Cheeseman IM (2015). The CENP-L-N complex forms a critical node in an integrated meshwork of interactions at the centromere-kinetochore interface. Mol Cell 60, 886–898.

Nagpal H, Hori T, Furukawa A, Sugase K, Osakabe A, Kurumizaka H, Fukagawa T (2015). Dynamic changes in CCAN organization through CENP-C during cell-cycle progression. Mol Biol Cell 26, 3768–3776.

Navarro AP, Cheeseman IM (2020). Chromosome segregation: evolving a plastic chromosome–microtubule interface. Curr Biol 30, R174–R177.
Navarro AP, Cheeseman IM (2021). Kinetochore assembly throughout the cell cycle. Semin Cell Dev Biol.
Nishino T, Takeuchi K, Gascoigne KE, Suzuki A, Hori T, Oyama T, Morikawa K, Cheeseman IM, Fukagawa T (2012). CENP-T-W-S-X forms a unique centromeric chromatin structure with a histone-like fold. Cell 148, 487–501.
Okada M, Cheeseman IM, Hori T, Okawa K, McLeod IX, Yates JR 3rd, Desai A, Fukagawa T (2006). The CENP-H-I complex is required for the efficient incorporation of newly synthesized CENP-A into centromeres. Nat Cell Biol 8, 446–457.
Pekgoz Altunkaya G, Malvezzi F, Demianova Z, Zimniak T, Litos G, Weissmann F, Mechtler K, Herzog F, Westermann S (2016). CCAN assembly configures composite binding interfaces to promote cross-linking of Ndc80 complexes at the kinetochore. Curr Biol 26, 2370–2378.
Pentakota S, Zhou K, Smith C, Maffini S, Petrovic A, Morgan GP, Weir JR, Vetter IR, Musacchio A, Luger K (2017). Decoding the centromeric nucleosome through CENP-N. eLife 6, e33442.
Pesenti ME, Prumbaum D, Auckland P, Smith CM, Faesen AC, Petrovic A, Erent M, Maffini S, Pentakota S, Weir JR, *et al*. (2018). Reconstitution of a 26-subunit human kinetochore reveals cooperative microtubule binding by CENP-OPQUR and NDC80. Mol Cell 71, 923–939.e910.
Pesenti ME, Raisch T, Conti D, Walstein K, Hoffmann I, Vogt D, Prumbaum D, Vetter IR, Raunser S, Musacchio A (2022). Structure of the human inner kinetochore CCAN complex and its significance for human centromere organization. Mol Cell 82, 2113–2131.e2118.
Saitoh H, Tomkiel J, Cooke CA, Ratrie H 3rd, Maurer M, Rothfield NF, Earnshaw WC (1992). CENP-C, an autoantigen in scleroderma, is a component of the human inner kinetochore plate. Cell 70, 115–125.
Schonenberger F, Deutzmann A, Ferrando-May E, Merhof D (2015). Discrimination of cell cycle phases in PCNA-immunolabeled cells. BMC Bioinformatics 16, 180.
Screpanti E, De Antoni A, Alushin GM, Petrovic A, Melis T, Nogales E, Musacchio A (2011). Direct binding of Cenp-C to the Mis12 complex joins the inner and outer kinetochore. Curr Biol 21, 391–398.
Sharma K, D'Souza RC, Tyanova S, Schaab C, Wisniewski JR, Cox J, Mann M (2014). Ultradeep human phosphoproteome reveals a distinct regulatory nature of Tyr and Ser/Thr-based signaling. Cell Rep 8, 1583–1594.
Songyang Z, Blechner S, Hoagland N, Hoekstra MF, Piwnica-Worms H, Cantley LC (1994). Use of an oriented peptide library to determine the optimal substrates of protein kinases. Curr Biol 4, 973–982.
Tian T, Li X, Liu Y, Wang C, Liu X, Bi G, Zhang X, Yao X, Zhou ZH, Zang J (2018). Molecular basis for CENP-N recognition of CENP-A nucleosome on the human kinetochore. Cell Res 28, 374–378.
van den Berg J, G.M. A, Kielbassa K, Feringa FM, Freire R, Medema RH (2018). A limited number of double-strand DNA breaks is sufficient to delay cell cycle progression. Nucleic Acids Res 46, 10132–10144.
Wang T, Birsoy K, Hughes NW, Krupczak KM, Post Y, Wei JJ, Lander ES, Sabatini DM (2015). Identification and characterization of essential genes in the human genome. Science 350, 1096–1101.
Watanabe R, Hara M, Okumura EI, Herve S, Fachinetti D, Ariyoshi M, Fukagawa T (2019). CDK1-mediated CENP-C phosphorylation modulates CENP-A binding and mitotic kinetochore localization. J Cell Biol 218, 4042–4062.
Weir JR, Faesen AC, Klare K, Petrovic A, Basilico F, Fischbock J, Pentakota S, Keller J, Pesenti ME, Pan D, *et al*. (2016). Insights from biochemical reconstitution into the architecture of human kinetochores. Nature 537, 249–253.
Yatskevich S, Muir KW, Bellini D, Zhang Z, Yang J, Tischer T, Predin M, Dendooven T, McLaughlin SH, Barford D (2022). Structure of the human inner kinetochore bound to a centromeric CENP-A nucleosome. Science 376, 844–852.